Band-Gap Engineering of Metal Oxides for Dye-Sensitized Solar Cells

M. Dürr,* S. Rosselli, A. Yasuda, and G. Nelles†

Materials Science Laboratory, Sony Deutschland GmbH, 70327 Stuttgart, Germany

Received: June 20, 2006; In Final Form: September 1, 2006

Mixed oxides $Ti_{1-x}Zr_xO_2$ with $0 < x \leq 0.2$ were synthesized by means of thermal hydrolysis for use in dye-sensitized solar cells. The lattice parameter *d* is observed to increase linearly with Zr content *x*. The band gap of the mixed oxides was measured to increase by up to 0.2 eV. The respective shift of the conduction band edge leads to an increase of the open circuit voltage (V_{OC}) by up to 0.1 V. Among others, temperature-dependent measurements of V_{OC} clearly identify the correlation between band edge shift and change in V_{OC}.

Introduction

Metal-oxide semiconductors, especially TiO_2, are intensively used both in electrochemical and in photoelectrochemical applications.[1−3] Because of their large internal surface area, porous media are of special interest for high turnover applications. With respect to photoelectrochemical applications, light is either directly absorbed by the TiO_2, or the semiconductor material serves as an electron conductor for electrons injected from dye molecules, which are adsorbed on its surface. The latter concept finds its application, for example, in dye-sensitized solar cells (DSSC). In these cells, the dye molecule is regenerated from a second electrode via a redox couple in electrolyte, and a photovoltaic current is established between the TiO_2- and the counter-electrode.[4]

In both kinds of application, that is, direct absorption or dye-sensitization, the exact positions of the band edges play a decisive role for the efficiency of the respective process. For direct excitation in the semiconductor, the band positions determine the band gap and therefore the threshold energy of the absorbed photons. In the case of dye-sensitization, the conduction band (CB) edge has to match the lowest excited state of the dye molecule to enable effective electron transfer from the molecule's excited state to the semiconductor's conduction band. If the CB edge is too high in energy, that is, higher than the excited state of the dye molecules, electron injection from the dye into the conduction band is suppressed. If, on the other hand, the CB level is low in energy, the electron injection might be good. However, the electrons lose energy by means of thermalization in the CB, which is then lost for further photovoltaic energy conversion. In the case of DSSC, this shows up as a reduced open circuit voltage (V_{OC}) because V_{OC} is, among others, determined by the energy difference between CB edge and redox potential of the ion conductor.

It is therefore highly desirable to design semiconductors with tunable band edge positions and band gap. In this contribution, we describe such band-gap engineering by means of the synthesis of nanoporous titanium−zirconium mixed oxides. As indicated in Figure 1, the band edge positions of $Ti_{1-x}Zr_xO_2$ are expected to change with the content of zirconium, *x*, between the positions of TiO_2 and ZrO_2, similar to earlier observed band edge movement in mixed oxide systems, for example, in ref 6.

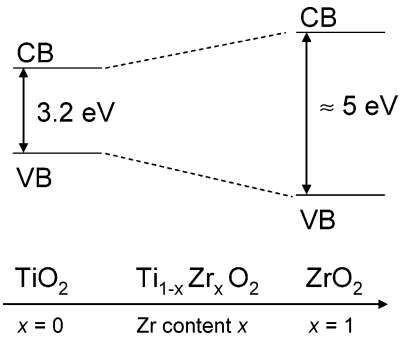

Figure 1. Schematics of the dependence of conduction band edge and valence band (VB) edge as a function of zirconium content *x* in a mixed oxide. Band offsets are chosen similarly to the results in ref 5.

An increase of zirconium content should therefore allow for a higher CB edge and, in consequence, for a higher open circuit voltage when used in DSSC. Indeed, very recently it was shown for one fixed value of zirconium content, $x = 5\%$, that an increase in open circuit voltage can be achieved.[7]

In this contribution, we studied systematically the electrical properties of $Ti_{1-x}Zr_xO_2$ as a function of *x* and especially their influence on the photovoltaic properties of the dye-sensitized solar cells. Additionally, the effect of zirconium content on lattice structure and the optical properties of the nanoparticles have been studied. Indeed, a monotone increase of lattice constant and open circuit voltage was observed with increasing zirconium content. The latter was traced back to the change of the band edge positions. A widened band gap was directly observed by means of UV−vis spectroscopy.

Experimental Section

Materials. The synthesis of mixed oxide particles was performed as follows: $(1 - x)$ mole of titanium isopropoxide, $Ti(^iPrO)_4$ (Aldrich), was mixed with an equimolar amount of acetic acid, CH_3COOH (VWR). The mixture was stirred until a pale yellow color appeared. Then *x* mole of zirconium isopropoxide, $Zr(^iPrO)_4$ (Aldrich), was added. The mixture was poured under continuous stirring into a beaker containing distilled water. The resulting milky mixed oxide suspension was heated at 80 °C in the presence of HNO_3 (0.1 M, VWR). Finally, the mixture was poured into a Teflon inlet inside a stainless steel reactor and heated at 240 °C for 12 h.

DSSC Preparation. The DSSC were assembled as follows: A 30-nm-thick bulk TiO_2 blocking layer was formed on FTO

* Corresponding author. Present address: University of Applied Sciences Esslingen. E-mail: Michael.Duerr@hs-esslingen.de.
† E-mail: Nelles@sony.de.

10.1021/jp063857c CCC: $33.50 © 2006 American Chemical Society
Published on Web 10/10/2006

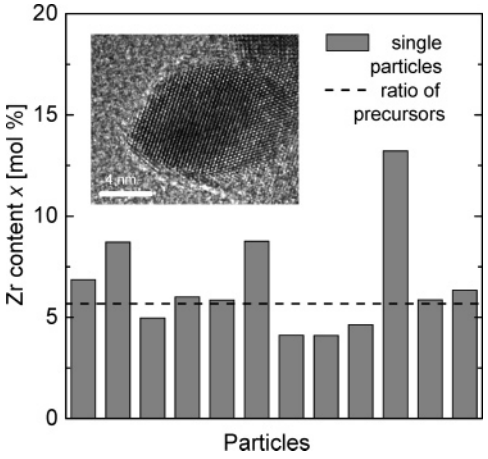

Figure 2. Zr content as measured by EDX for 12 single particles synthesized with a $Zr(^iPrO)_4$ content of $x = 5.7\%$. Inset: TEM image of particles made by the same synthesis.

(approximately 100 nm on glass). An approximately 10-μm-thick porous layer of semiconductor particles was screen printed on the blocking layer and sintered at 450 °C for half an hour. If not mentioned otherwise, red-dye (*cis*-bis(isothiocyanato)-bis(2,2′-bipyridyl-4,4′-dicarboxylic acid) ruthenium(II)) molecules were adsorbed to the particles via self-assembling out of a solution in ethanol (0.3 mM), and the porous layer was filled with electrolyte containing I^-/I_3^- as redox couple with $c(I_3^-) = 15$ mM. A reflective platinum back electrode was attached with a distance of 6 μm from the porous layer.

Characterization. Transmission electron microscopy (TEM) and energy-dispersive X-ray (EDX) analysis were performed using a TECNAI G2 F20 transmission electron microscope from FEI. X-ray diffraction studies exploited the K_α line of a copper anode with a wavelength $\lambda = 1.54$ Å. The lattice spacing d was then calculated via $\lambda/d = 2 \sin \theta/2$. External quantum efficiency measurements were performed at constant light intensity of 2 mW/cm^2. Current−voltage characteristics were taken under illumination with white light from a sulfur lamp, and the intensity was 100 mW/cm^2.

Results and Discussion

Pure TiO_2 and mixed oxide was synthesized by means of thermal hydrolysis starting from either the pure TiO_2 precursor, that is, titanium isopropoxide, $Ti(^iPrO)_4$, or a mixture of $Ti(^iPrO)_4$ and zirconium isopropoxide, $Zr(^iPrO)_4$, respectively. The ratio of the precursors was found to determine the atomic composition on the nanoparticles' scale. This is documented in Figure 2, where a typical transmission electron micrograph of mixed oxide particles is depicted together with the atomic ratio of Zr and Ti in 12 single particles as determined by means of energy-dispersive X-ray analysis (EDX). A good match between the initial ratio of the precursors and the ratio of the metal ion in the particles is observed. The reproduction of the ratio of the precursors in the mixed oxide particles was also confirmed on the macroscopic scale by means of X-ray photoelectron spectroscopy (XPS).

Furthermore, X-ray diffraction (XRD) measurements of the mixed oxide material show that for lower Zr content the Zr atoms are distributed homogeneously in the nanoparticles. As shown in Figure 3, the anatase structure of TiO_2 prevails in the case of the mixed oxides. A more detailed analysis of the XRD data from Figure 3 shows that the peak maxima shift toward smaller angles when the Zr content is increased. As an example, the peak at $2\theta \cong 25°$ is shown both for pure TiO_2 as well as

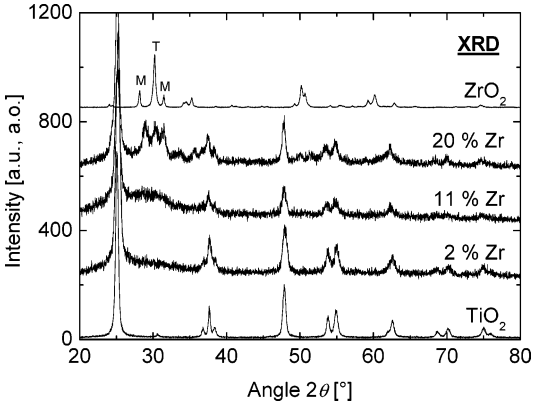

Figure 3. XRD diffractograms of TiO_2 anatase and mixed oxides with various Zr content x. For comparison, a diffractogram of ZrO_2 is shown. The peaks of the latter one can be attributed to the monoclinic (M) and tetragonal (T) phase as exemplified for $2\theta \approx 30°$.

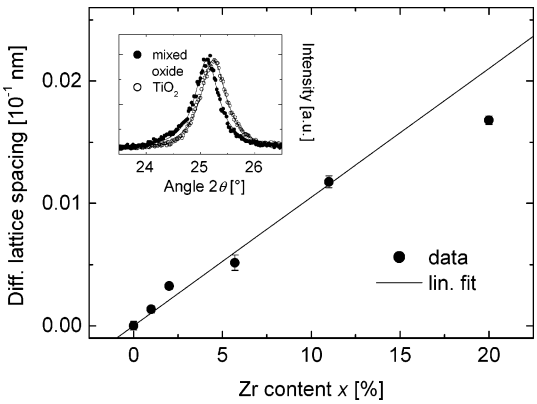

Figure 4. Change in lattice spacing of mixed oxides with respect to TiO_2 as obtained from the evaluation of the XRD data shown in the inset (Zr content in mixed oxide of inset was 20%). For the linear fit, only the data of the lowest five values of Zr content were taken into account.

for mixed oxide with 20% Zr content in Figure 4, inset. This behavior clearly indicates that most of the Zr atoms are evenly distributed in the whole nanocrystal. Otherwise, for example, in the case of a core−shell formation with TiO_2 as core and ZrO_2 as shell material, no such change in the peak position of the TiO_2 anatase should be observed. For a quantitative analysis, the maximum of the single peaks is determined by fitting Lorentz-shaped curves to the data, and the respective change in lattice constant is depicted in Figure 4. One observes a linear relationship between the increasing lattice constant and the content of Zr atoms in the mixed oxide, in good agreement with Vegard's law.[8,9] Only at 20% Zr content, the measured lattice spacing deviates from this linear behavior. This is in accordance with the observation that, starting from 11% of Zr content, additional features appear in the XRD diffractogram of the mixed oxides around $2\theta \cong 30°$. Most likely, they origin from smaller segregations with a majority of ZrO_2 as a comparison with data of pure ZrO_2 suggests.[10,11] As a consequence, the actual Zr content in the Ti-rich phase of the mixed oxide is smaller than 20%, leading to a lower increase of the lattice spacing.

The increased Zr content does not only account for the increased lattice constant but also for a larger band gap in accordance with the scenario depicted in Figure 1. Experimental evidence is obtained from UV−vis spectroscopy of both TiO_2 and mixed oxide layers. For the latter one, the onset of absorption starts at lower wavelengths. For example, two spectra are shown in the inset of Figure 5, both for pure TiO_2 and for a mixed oxide with $x = 0.2$. From the different threshold for

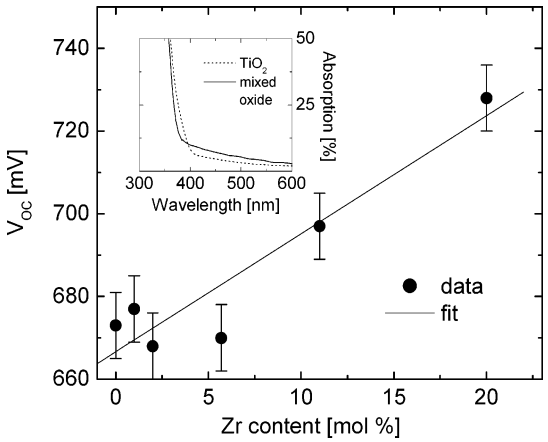

Figure 5. Open circuit voltage V_{OC} of DSSC as a function of Zr content in the mixed oxide and linear fit to the data; each value represents the averaged results of three cells from a single, representative data set, and error bars are calculated from the standard deviation. Inset: Total absorption of 2-μm-thick films as measured by means of an integrating sphere for both TiO_2 and $Ti_{0.8}Zr_{0.2}O_2$.

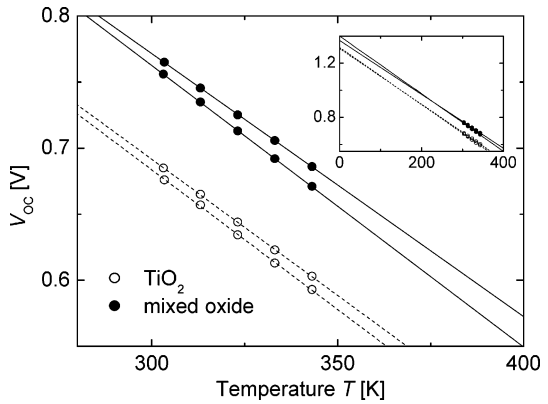

Figure 6. Open circuit voltage V_{OC} as a function of temperature T for cells both made from TiO_2 and made from $Ti_{0.8}Zr_{0.2}O_2$ (two samples each). The linear fits show a similar slope for all cells. Inset: Zoom-out of the same data.

absorption, an increase of the band gap by approximately 0.2 eV was derived. If one assumes a similar shift of both the valence band edge and the conduction band edge,[5] then both should move by about 0.1 eV, which sets the upper limit for the change in V_{OC}. Indeed, an increase of V_{OC} by up to 80 mV for DSSC made from mixed oxide when compared to pure TiO_2 was observed (Figures 5 and 6). A closer look at Figure 5 reveals that, at low Zr content, the effect of the band widening on V_{OC} is not so pronounced; up to a Zr content of nominally 5.7%, not much change of V_{OC} is observed. However, at this point it should be noted that V_{OC} is not only dependent on the energy difference between conduction band minimum and redox potential of the redox couple I^-/I_3^-. Recombination losses between electrons in the conduction band and tri-iodide of the electrolyte can additionally decrease V_{OC}.[12−14] A changed surface morphology and additional recombination channels may therefore (over)compensate for the effect of band-gap widening in the case of lower Zr content in the mixed oxides.

To further strengthen our argumentation on the relationship between Zr content, band position, and open circuit voltage, two additional experiments were performed. First, the dependence of V_{OC} on temperature T was measured as displayed in Figure 6. The data for the cells with mixed oxide are in general higher but show the same linear dependence on temperature as the cells with pure TiO_2. This behavior is indeed indicative of

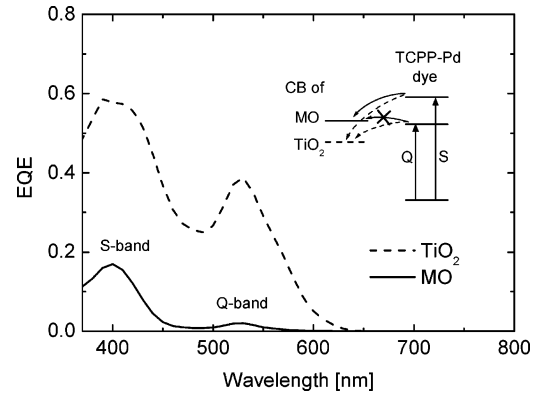

Figure 7. External quantum efficiency EQE as a function of irradiating wavelength for TCPP-Pd colored layers of TiO_2 and mixed oxide (MO, $x = 20\%$). Inset: Schematics of the energy levels (not to scale).

a change in band positions rather than a changed recombination rate. A reduced recombination rate causes a different slope of $V_{OC}(T)$, whereas a change in band positions leads to a change in $V_{OC}(T = 0\ K)$ but the temperature dependence stays unchanged.[13,14] The latter behavior is even better observed when extrapolating the data to $T = 0$ K, as shown in the inset of Figure 6.

Second, external quantum efficiency (EQE) measurements are shown in Figure 7. The shift of the conduction band minimum does not only change the open circuit voltage but also influences the injection efficiency from the excited state of the dye molecules to the conduction band of the semiconductor because the energy difference is the main driving force for this mechanism.[15] One therefore observes in general a lower short circuit current density the higher the conduction band minimum is located.[16] This is also observed for the mixed oxides of this contribution. Additionally, external quantum efficiency measurements with porous layers stained with porphyrin dye molecules (5,10,15,20-tetrakis(4-carboxyphenyl)-porphyrin-Pd(II), short: TCPP-Pd) directly image the shift of the conduction band edge. The EQE spectra of the TCPP-Pd colored TiO_2 layers in Figure 7 show two maxima around 530 and 400 nm due to the absorption of the first two electronic excitations of the TCPP-Pd, that is, the Q-band and the S-band, respectively.[17] For TiO_2, the ratio between the two maxima is about 1.5, in agreement with previous investigations.[17] For the mixed oxide, however, one observes not only an in general lower intensity but the ratio between the two EQE maxima is increased by a factor of 5. As illustrated in the inset of Figure 7, this clearly indicates that the conduction band edge of the mixed oxide is shifted toward higher values: such a shift affects the injection from the lower excited state (Q-band) much more than injection from the higher excited state (S-band).

With respect to power conversion efficiency, we observe improvements only for the DSSC with mixed oxides of low Zr content, $x = 1\%$ (Figure 8). With higher Zr content and therefore higher conduction band minimum, we observe a drop in short circuit current density due to the reduced driving force for electron injection into the semiconductor, which cannot be compensated by the higher V_{OC}. The photovoltaic parameters taken from the best cells' data set compare as follows: for the best cell based on pure TiO_2, we measured $J_{SC} = 15.6$ mA/cm^2, $V_{OC} = 700$ mV, and fill factor $FF = 0.64$, which results in a power conversion efficiency of 7.0%, whereas for the best cell based on mixed oxide we measured $J_{SC} = 16.5$ mA/cm^2, $V_{OC} = 715$ mV, $FF = 0.69$ and a resulting power conversion efficiency of 8.1%. Both porous layers were measured to be 8 μm thick. In addition to the increased V_{OC} due to the shift of the conduction

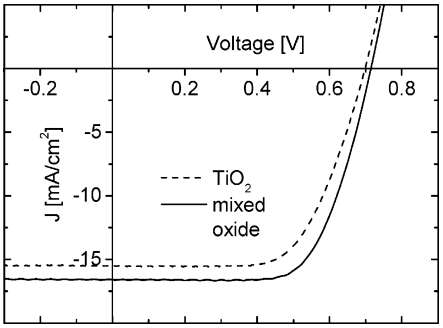

Figure 8. *J*−*V* characteristics of DSSC with porous layers consisting both of pure TiO_2 and of mixed oxide with 1% Zr content. Active area was 0.24 cm^2.

gap of the mixed oxide, an increase in J_{SC} is observed, which is attributed to a slight increase of internal surface area from 86 m^2/g for the pure TiO_2 material to 97 m^2/g for the mixed oxide, in agreement with ref 7. The higher *FF* might be also associated with the changed morphology of the nanoporous film. Differences in the diffusion pathways through the nanoporous network can lead to a reduced resistivity of the film and hence an increased *FF*.[18]

In summary, we could show that the use of mixed Ti−Zr oxides in DSSC leads to an increasing open circuit with increasing Zr content *x*. It was traced back to a shift of the conduction band edge toward higher energies. Improved power conversion efficiency was found for small content of Zr. Toward higher values of *x*, the reduced electron injection due to the higher conduction band causes a drop in power conversion efficiency. Nonetheless, the presented results have some importance with respect to further improvements of DSSC. Current dye molecules are optimized for the combination with TiO_2; however, the successful demonstration of mixed oxides in DSSC might trigger new dye synthesis with respect to these new materials. Especially with respect to tandem solar cell concepts, which aim toward a better use of the full sun spectrum,[19,20] one can easily think of an optimization of one or both of the compartments with the help of band-gap engineered semiconductors. For example, the compartment that uses dyes absorbing in the shorter wavelength region might be combined with semiconductors with a wider band gap. The so far widely unemployed longer wavelength region of the solar spectrum becomes then more easily accessible when a semiconductor with lower CB minimum and a dye absorbing in the longer wavelength region is chosen in a further compartment.

Acknowledgment. We would like to thank Michael Steiert for the XRD measurements, as well as A. Bamedi, G. Fuhrmann, and M. Obermaier for fruitful discussions and experimental help.

Note Added after Print Publication. Due to a production error, the corresponding author's e-mail address was incorrect in the original published version of this article (Web 10/10/2006; print Volume 110, No. 43, pp 21899−21902). The corrected electronic version was reposted on November 22, 2006 and an Addition and Correction appears in the December 28, 2006 issue (Vol. 110, No. 51).

References and Notes

(1) Fujishima, A.; Honda, K. *Nature* **1972**, *238*, 37.
(2) Linsebigler, A. L.; Lu, G.; Yates, J. T. *Chem. Rev.* **1995**, *95*, 735.
(3) Fujishima, A.; Rao, T. N.; Tryk, D. A. *J. Photochem. Photobiol., C* **2000**, *1*, 1.
(4) Grätzel, M. *Nature* **2001**, *414*, 338.
(5) Puthenkovilakam, R.; Chang, J. P. *Appl. Phys. Lett.* **2004**, *84*, 1353.
(6) Nagaveni, K.; Hedge, M. S.; Madras, G. *J. Phys. Chem. B* **2004**, *108*, 20204.
(7) Kitiyanan, A.; Ngamsinlapasathian, S.; Pavasupree, S.; Yoshikawa, S. *J. Solid State Chem.* **2005**, *178*, 1044.
(8) Vegard, L. *Z. Phys.* **1921**, *5*, 17.
(9) Denton, A. R.; Ashcroft, N. W. *Phys. Rev. A* **1991**, *43*, 3161.
(10) Noh, H.-J.; Seo, D.-S.; Kim, H.; Lee, J.-K. *Mater. Lett.* **2003**, *57*, 2425.
(11) Manríquez, M. E.; López, T.; Gómez, R.; Navarrete, J. *J. Mol. Catal. A* **2004**, *220*, 229.
(12) Nazeeruddin, M. K.; et al. *J. Am. Chem. Soc.* **1993**, *115*, 6382.
(13) Kron, G.; Egerter, T.; Werner, J. H.; Rau, U. *J. Phys. Chem. B* **2003**, *107*, 3556.
(14) Dürr, M.; Yasuda, A.; Nelles, G. *Appl. Phys. Lett.* **2006**, *89*, 061110.
(15) Wang, Z.-S.; Yamaguchi, T.; Sugihara, H.; Arakawa, H. *Langmuir* **2005**, *21*, 4272.
(16) Moser; et al. *Z. Phys. Chem.* **1999**, *212*, 85.
(17) Dürr, M.; et al. *Proc. 19th EPSEC* **2004**, *1*, 21.
(18) Dürr, M.; Schmid, A.; Obermaier, M.; Rosselli, S.; Yasuda, A.; Nelles, G. *Nat. Mater.* **2005**, *4*, 607.
(19) Dürr, M.; Bamedi, A.; Yasuda, A.; Nelles, G. *Appl. Phys. Lett.* **2004**.
(20) Shevaleevskiy, O.; Larina, L.; Lim, K.-S. *Proc. 15th PVSEC* **2005**, *2*, 754.